Article

Damping Characteristics of Ti$_{50}$Ni$_{50-x}$Cu$_x$ (*x* = 0~30 at.%) Shape Memory Alloys at a Low Frequency

Chen Chien [1], Shyi-Kaan Wu [1,2],* and Shih-Hang Chang [3]

[1] Department of Materials Science and Engineering, National Taiwan University, No. 1, Sec. 4, Roosevelt Road, Taipei 106, Taiwan; E-Mail: d01527004@ntu.edu.tw

[2] Department of Mechanical Engineering, National Taiwan University, No. 1, Sec. 4, Roosevelt Road, Taipei 106, Taiwan

[3] Department of Chemical and Materials Engineering, National I-Lan University, No. 1, Sec. 1, Shen-Lung Road, I-Lan 260, Taiwan; E-Mail: shchang@niu.edu.tw

* Author to whom correspondence should be addressed; E-Mail: skw@ntu.edu.tw; Tel.: +886-2-2363-7846; Fax: +886-2-2363-4562.

Abstract: The damping characteristics of Ti$_{50}$Ni$_{50-x}$Cu$_x$ (*x* = 0~30 at.%) shape memory alloys (SMAs) at a low frequency have been studied using a dynamic mechanical analyzer. The magnitude of the tan δ value and the values of the storage modulus (E_0) softening/hardening and the strain variation exhibited in B2↔B19 transformation are all higher than those in B2↔B19' transformation. The larger E_0 softening/hardening in B2↔B19 can induce higher strain variation in this transformation. It is suggested that the greater mobility of the twin boundaries and the larger magnitude of the strain variation both cause the higher tan δ value exhibited in B2↔B19 transformation, as compared with B2↔B19' transformation. In comparison with that in B19' martensite, the E_0 value in B19 martensite is low and not affected so greatly by changes in temperature. Relaxation peaks are observed in B19' martensite, but not in B19 martensite, because the latter has rare twinned variants. The activation energy of the relaxation peak is calculated and found to increase as the Cu-content increases in these SMAs.

Keywords: shape memory alloys; damping properties; martensitic transformation; twins; relaxation peak

1. Introduction

TiNi shape memory alloys (SMAs), which undergo thermoelastic martensitic transformation can exhibit good shape memory effect (SME), pseudoelasticity (PE), and high damping capacity [1–8]. The addition of Cu into TiNi SMAs improves the SME and PE properties and reduces the temperature hysteresis of the SMAs [9,10]. It has been reported that the transformation sequences of $Ti_{50}Ni_{50-x}Cu_x$ (x = 0~30 at.%) SMAs are B2↔B19', B2↔B19↔B19' and B2↔B19, when the Cu-contents are $x \leq 7.5$, $10 \leq x \leq 15$ and $20 \leq x \leq 30$, respectively [11–13]. The damping properties exhibited in TiNiCu SMAs can be examined with a dynamic mechanical analyzer (DMA). However, the phenomena of the storage modulus (E_0) softening/hardening and the magnitude of the tan δ value exhibited in TiNiCu SMAs during B2↔B19' and B2↔B19 martensitic transformations have not been clarified. In addition, a broad peak appears at around −70 °C in the DMA curve of TiNi/TiNiCu SMAs [14]. This broad peak, which does not correspond to E_0 softening/hardening, is called the relaxation peak. However, the effect of the Cu-content of $Ti_{50}Ni_{50-x}Cu_x$ SMAs on the occurrence of the relaxation peak is not fully understood In this study, we examine the tan δ value and the E_0 softening/hardening associated with B2↔B19' and B2↔B19 transformations in $Ti_{50}Ni_{50-x}Cu_x$ (x = 0~30 at.%) SMAs. The damping properties exhibited in B19' martensite are compared with those in B19 martensite. The effect of the Cu-content in $Ti_{50}Ni_{50-x}Cu_x$ SMAs on occurrence of the relaxation peak and its activation energy (E_a) are also discussed.

2. Results and Discussion

2.1. Tan δ Value versus Temperature (T)

As mentioned in Section 2, DMA tests were conducted at a low frequency of 1 Hz and a cooling rate of 3 °C/min (instead at the isothermal condition, *i.e.*, at 0 °C/min), thus, the obtained tan δ values are mostly contributed by the transitory term (IF_{Tr}) [12,15,16]. Figure 1a–c show the tan δ value *versus* T curves for $Ti_{50}Ni_{50-x}Cu_x$ (x = 0, 5, 7.5 at.%) SMAs, respectively. According to the reported transformation sequence[11–13], Figure 1a indicates a B2 →B19' transformation peak appearing at 24 °C with a tan δ value of 0.11 in cooling, and a B19'→B2 transformation peak occurring at 78 °C with a tan δ value of 0.09 in heating. Figure 1b,c show the same transformation peaks as Figure 1a. The peak temperature and its tan δ value are found to decrease as the Cu-content increases. Figure 1 reveals that there is a transformation peak appearing in the cooling/heating curve which is regarded as a B2↔B19' transformation exhibited in SMAs when the Cu-content is below 7.5 at.%. In addition, there are relaxation peaks at about −70 °C and −50 °C in cooling and heating, respectively. The studies of electric resistivity, ρ, and Seebeck coefficient, S, *versus* T for $Ti_{50}Ni_{50-x}Cu_x$ (x = 0~30 at.%) SMAs demonstrate that the transformation sequence exhibited in x = 7.5 at.% SMA is B2↔B19' by ρ tests and is B2↔B19↔B19' with $M_S' - M_S$ = 15 °C by S tests [11]. Here, $M_S'$and M_S are the starting transformation temperatures of B2→B19 and B19→B19', respectively. The DSC curves for x = 7.5 at.% SMA also show only a B2↔B19' peak in cooling and heating [17]. Obviously, the DMA curves for x = 7.5 at.% SMA, as shown in Figure 1c, cannot be used to distinguish the B19 martensite from B2↔B19' transformation, as revealed in ρ and DSC tests.

Figures 2a–c and 3a–c show the tan δ value *versus T* curves for *x* = 10, 12.5, 15 at.%, and *x* = 20, 25, 30 at.%, respectively. The former demonstrates a two-stage B2↔B19↔B19' transformation, and the latter shows an one-stage B2↔B19 transformation, which are both consistent with those reported in previous studies [12,18,19]. Figure 2 indicates that, at the peak temperature, the tan δ value is higher but the storage modulus (E_0) value is lower in B2↔B19 transformation than in B19↔B19' transformation. At the same time, the tan δ peak is sharp for B2↔B19 transformation, but it is rather broad for B19↔B19' transformation. This feature may have resulted from the fact that the difference of the starting and finishing transformation temperatures for B2↔B19 is much smaller than that for B19↔B19' [11]. Figure 2 also reveals that, in cooling, B2→B19 transformation peaks have tan δ values of around 0.17, but the B2→B19' values shown in Figure 1 are only about 0.11. Note that the transformation hysteresis of the B2↔B19' transformation is larger than that of B2↔B19 transformation, as measured by the difference in the peaks' temperatures shown in Figures 1 and 3, respectively. In addition, no obvious relaxation peak is found in Figure 3. Therefore, from the viewpoint of the damping application at room temperature, the SMAs shown in Figure 2 are better. This is because there is a B2→B19 transformation peak appearing around the room temperature, which exhibits higher tan δ value than that for B2→B19' transformation.

The broad peaks at around −30 °C~−70 °C for *x* = 10, 12.5, 15 SMAs shown in Figure 2 are also tested in the f range of 0.5~100Hz to identify whether they are relaxation peaks or not. Experimental results show that the T_p of these broad peaks does not shift to higher temperatures when the applied frequency is increased. Therefore, these broad peaks are not relaxation peaks but B19↔B19' transformation peaks, for this transformation is an athermal process [20].

2.2. Storage Modulus Value (E_0) versus Temperature (T)

It is well known that the softening of the elastic shear constant occurs in the forward martensitic transformation of SMAs [21,22]. This characteristic is also implicated in the E_0 *versus T* curves shown in Figures 1–3. From these E_0 *versus T* curves, the values of the E_0 softening/hardening and the E_0 slope in B19 and B19' martensites are measured, and they are listed in Table 1. Here, the magnitude of the E_0 softening/hardening and the values of the E_0 slope in B19 and B19' martensites are defined in the schematic E_0 *versus T* curve shown in Figure 4. Table 1 shows that the magnitude of the E_0 softening in B2→B19 transformation is much larger than that in B2→B19' transformation for *x* > 0. The same behavior also occurred in the E_0 hardening associated with the reverse martensitic transformation. These features demonstrate that the E_0 softening/hardening exhibited in B2↔B19 transformation is more significant than that in B2↔B19' transformation.

Carefully examining Figures 1–3 reveals that the E_0 slope in B2 phase is positive, but those in B19 and B19' martensites are both negative. As shown in Figure 2a, for $Ti_{50}Ni_{40}Cu_{10}$ SMA, the value of the E_0 slope in B19 martensite is −85 MPa/°C, and that in B19' martensite is −329 MPa/°C. This indicates that the absolute value of the E_0 slope in B19' martensite is much higher than that in B19 martensite. This characteristic may imply that the magnitude of the elastic modulus in B19 martensite is less than that in B19' martensite. In addition, the E_0 value of B19 martensite does not change much as the temperature decreases, but it changes significantly in B19' martensite. As also can be seen from Table 1, the magnitude of E_0 softening is slightly less than that of E_0 hardening in B2↔B19' transformation, but

it is just the reverse in B2↔B19 transformation. This feature may be related to the insignificant E_0 softening/hardening occurred in B2↔B19' transformation.

Figure 1. The tan δ value and storage modulus (E_0) curves for Ti$_{50}$Ni$_{50-x}$Cu$_x$ SMAs. (**a**) $x = 0$; (**b**) $x = 5$; (**c**) $x = 7.5$ at.%. The blue number is the E_0 slope in B19' martensite, and the red numbers are the magnitude of E_0 softening and hardening.
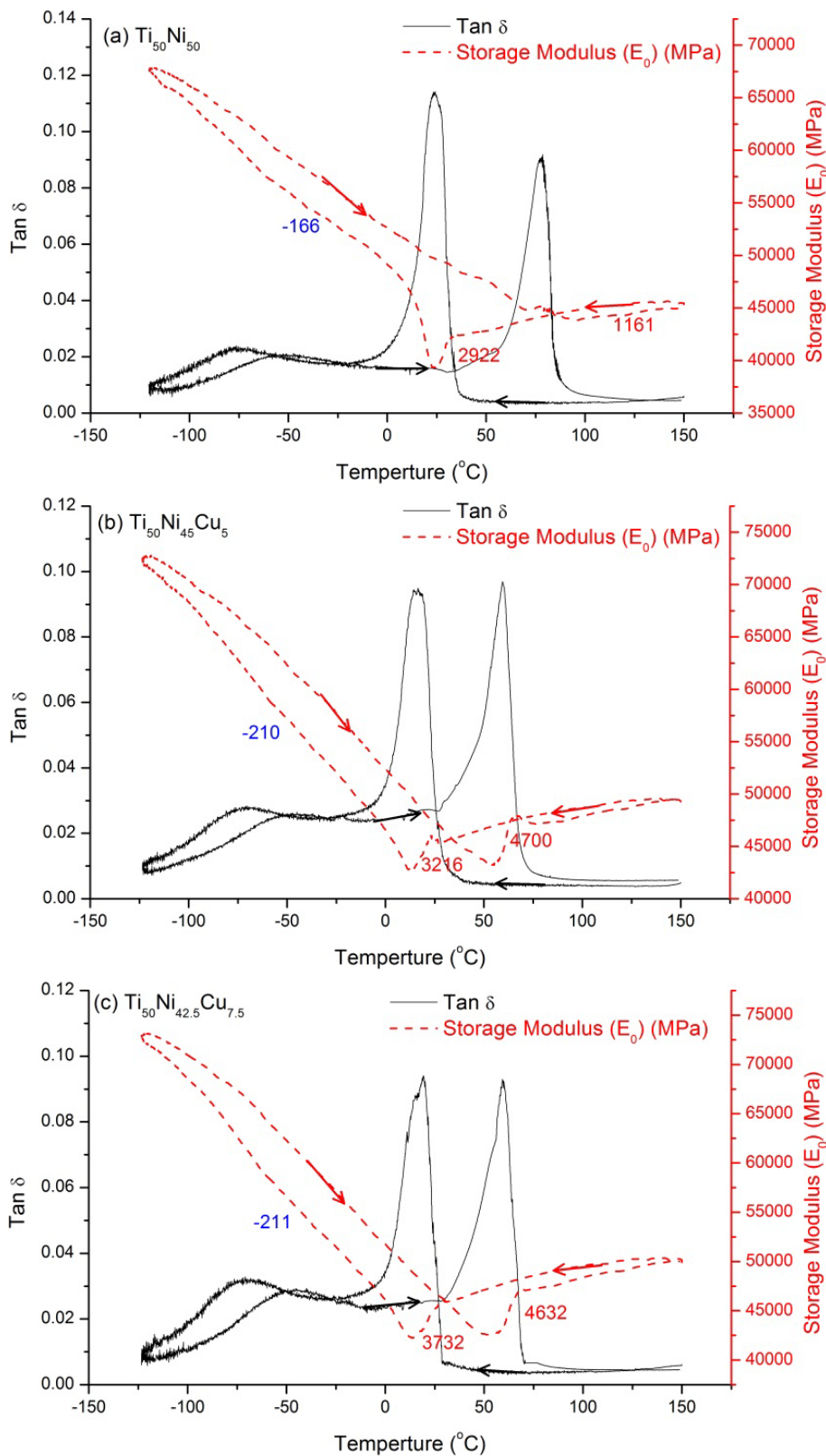
Figure 2. The tan δ value and storage modulus (E_0) curves for Ti$_{50}$Ni$_{50-x}$Cu$_x$ SMAs. (**a**) x = 10; (**b**) x = 12.5; (**c**) x = 15 at.%. The blue number are the E_0 slopes in B19' and B19 martensites, and the red numbers are the magnitude of E_0 softening and hardening.
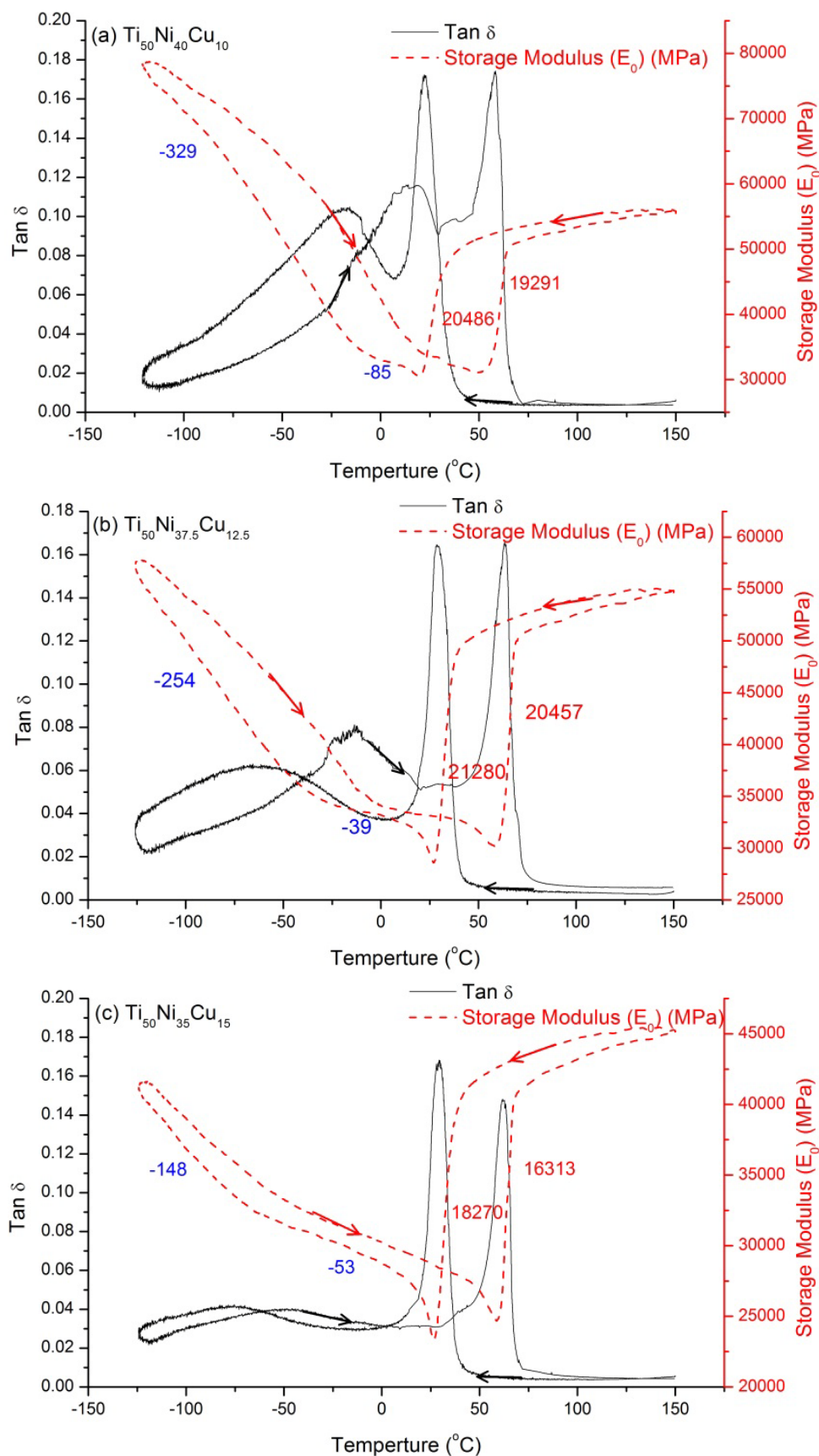
Figure 3. The tan δ value and storage modulus (E_0) curves for $Ti_{50}Ni_{50-x}Cu_x$ SMAs. (**a**) $x = 20$; (**b**) $x = 25$; (**c**) $x = 30$ at.%. The blue number is the E_0 slope in B19 martensite, and the red numbers are the magnitude of E_0 softening and hardening.
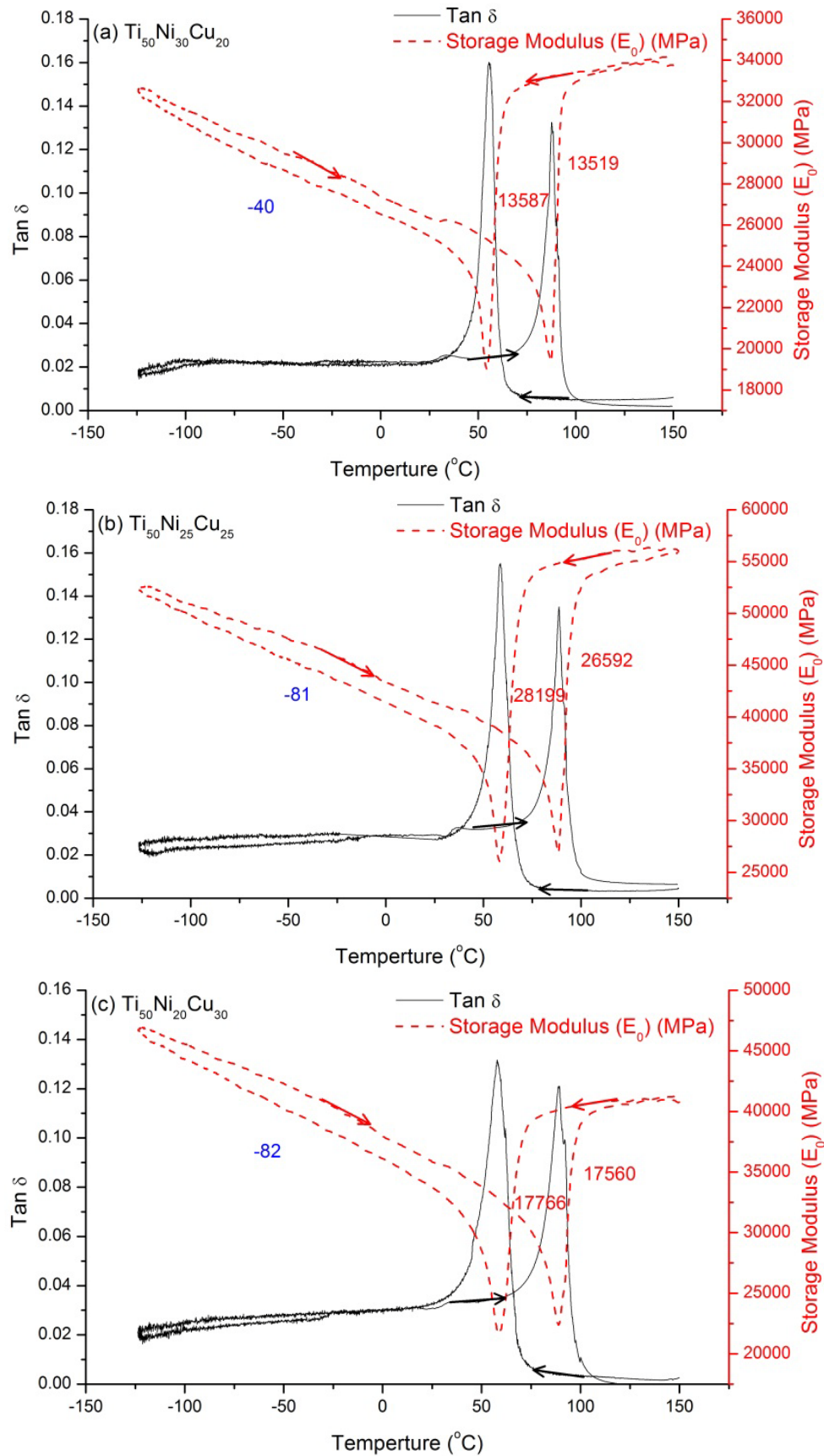
Table 1. Summary of the storage modulus (E_0) softening/hardening and the slope of E_0 *vs*. *T* curves in B19 and B19' martensites which are defined in the Figure 4.

$Ti_{50}Ni_{50-x}Cu_x$, *x* (at.%)	Transformation Sequences	E_0 softening (MPa)	E_0 hardening (MPa)	Slope of B19 (MPa/°C)	Slope of B19' (MPa/°C)
0		2922	1161	N/A	−166
5	B2↔B19'	3216	4700	N/A	−210
7.5		3732	4632	N/A	−211
10		20,486	19,291	−85	−329
12.5	B2↔B19↔B19'	21,280	20,457	−39	−254
15		18,270	16,316	−53	−148
20		13,587	13,519	−40	N/A
25	B2↔B19	28,199	26,592	−81	N/A
30		17,766	17,560	−82	N/A

Figure 4. The schematic diagram for the definitions of the storage modulus (E_0) softening/hardening and the slope of E_0 *vs*. *T*.
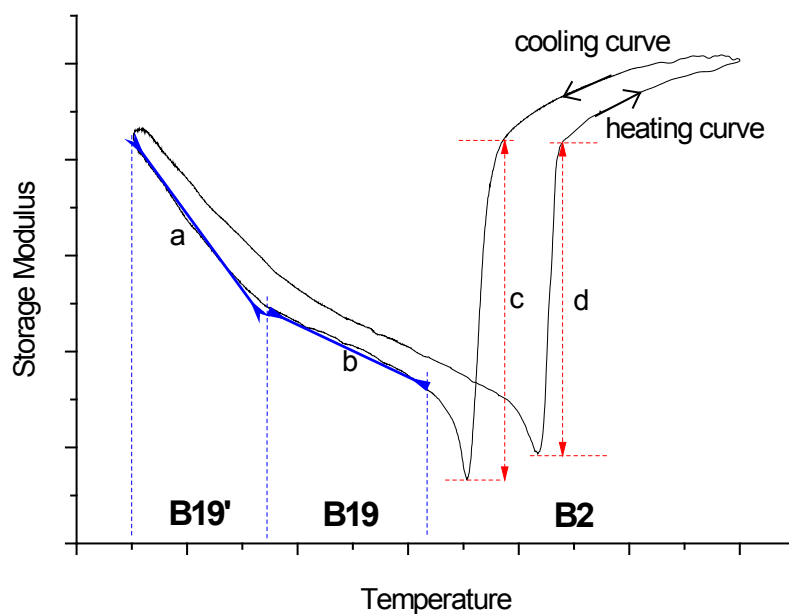

a: the E_0 slope in B19' martensite; b: the E_0 slope in B19 martensite; c: the magnitude of E_0 softening; d: the magnitude of E_0 hardening.

2.3. Strain Variation vs. Temperature (T)

Figure 5 show the curves of strain variation *versus* temperature (*T*) for $Ti_{50}Ni_{50-x}Cu_x$ SMAs with *x* = 0, 5, 15, 25 at.% in cooling and heating, respectively. In Figure 5, the upward and downward peaks correspond to the E_0 softening and hardening, respectively [23]. From Figure 5 and Table 1, it can be seen that the higher the E_0 softening/hardening is, the larger the strain variation is. From Figure 5, it can be found that the magnitude of the strain variation exhibited in B2↔B19 transformation is much higher than that in B2↔B19' transformation. This characteristic is ascribed to the fact that the former undergoes much higher E_0 softening/hardening than the latter during martensitic transformation.

Figure 5. The strain variation curves for $Ti_{50}Ni_{50-x}Cu_x$ SMAs, $x = 0, 5, 15, 25$ at.% (**a**) in cooling; (**b**) in heating.

(**a**)　　　　　　　　　　　　　(**b**)
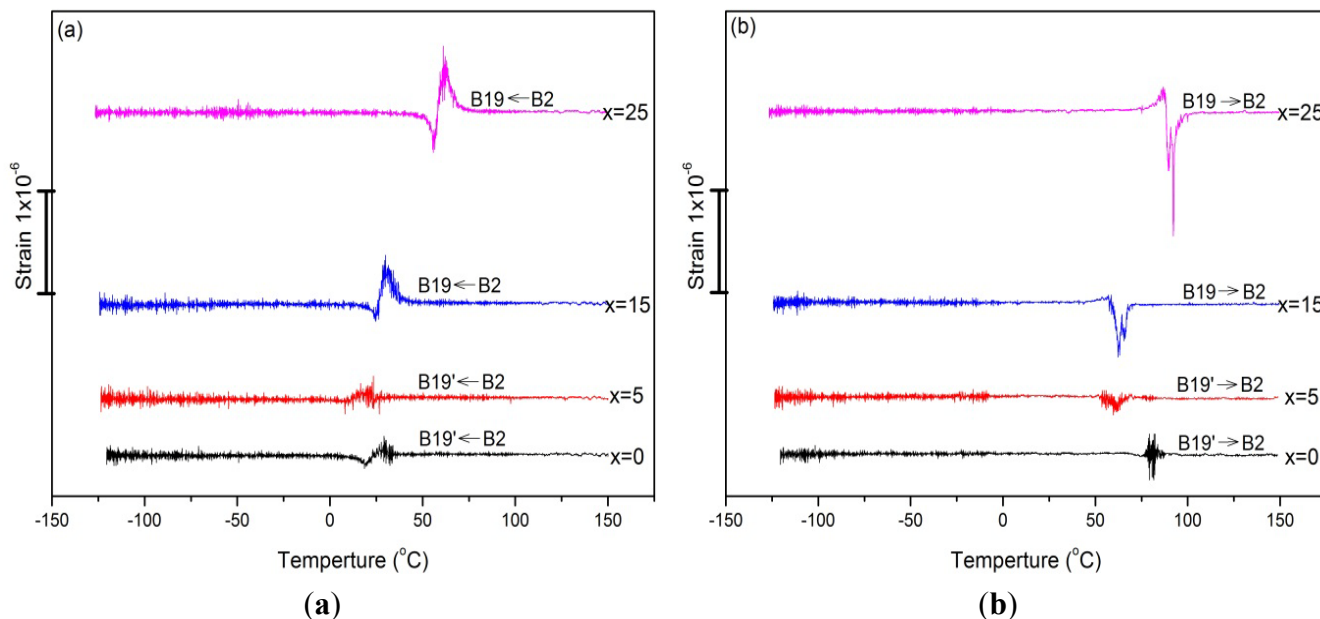
2.4. The Damping Properties Exhibited in B2↔B19 and B2↔B19' Transformations

It is interesting to clarify why the tan δ peak associated with B2↔B19 transformation is higher than that associated with B2 ↔B19' transformationAlthough the tan δ values in this study are most contributed from the transitory term (IF_{Tr}), as mentioned in Section 2.1, but from the strain sweep tests [17], we found that the phase transformation term (IF_{PT}) and the intrinsic term (IF_I) associated with B2↔B19 transformation are also higher than those associated with B2↔B19' transformation. The magnitude of the tan δ value exhibited by IF_{PT} term and that by IF_I term are closely related to the mobility of the phase interface between the parent phase and martensite and the twin boundary between the martensite variants. It has been reported that the twinning shear exhibited in B2→B19 transformation is smaller than that in B2→B19' transformation [19]. This characteristic also causes the twin boundaries between B19/B19 variants to move more easily than those in between B19'/B19' variants [19,24], and implicates that the interface between B2 and B19 phases is more mobile than that between B2 and B19' phases. In addition, as mentioned in Section 2.3, the magnitude of the E_0 softening/hardening during B2↔B19 transformation is greater than that during B2↔B19' transformation, which can induce higher strain variation in B2↔B19 transformation than in B2↔B19' transformation, as shown in Figure 5. It is suggested that the greater mobility of the twin boundaries (included phase interfaces) and the larger magnitude of the strain variation cause the higher tan δ value exhibited in B2↔B19 transformation than in B2↔B19' transformation.

2.5. The Relaxation Peak in DMA Curves

2.5.1. The Appearance of the Relaxation Peak

As mentioned in Section 2.1, the relaxation peaks are easy to obtain in Figure 1, but not in Figure 3. Ueura *et al.* [25] also found that, by DMA tests, the relaxation peak is absent in $Ti_{50}Ni_{50-x}Cu_x$ SMAs for

x = 15, 20 and 25 at.%, but it can be seen after these SMAs were hydrogen-doped in the concentration of 0.4~12 at.% H. It has been proposed that the origin of the relaxation peak is the hydrogen atoms pinning the twinned variants during the damping test [8]. The reported studies also indicate that most of the variants in B19 martensite are not twinned [26–28]. Therefore, the fact that no obvious relaxation peak is observed in Figure 3 implies that the twinned variants in B19 martensite is rare. Fan *et al*. [8] reported that the relaxation peaks were observed in B19 martensite in $Ti_{50}Ni_{34}Cu_{16}$ and $Ti_{50}Ni_{30}Cu_{20}$ SMAs. They found that, in B19 martensite, the twins will be induced to reduce the strain energy if the specimen is slowly cooled from B2 phase. Because, in reference [8], the DMA specimen was step-cooled during the test, in which the specimen was kept isothermally for 5 min at every 5 °C, it had enough time for twins to be introduced during B2→B19 transformation, and thus the relaxation peaks were induced in B19 martensite. However, in this study, the DMA specimen was continuously cooled (3 °C/min) at a rate faster than that in Reference [8]. Therefore, it is reasonable to propose that rare twinned variants are induced in the B19 martensite, thus explaining the absence of obvious relaxation peaks in Figure 3.

2.5.2. The Activation Energy (E_a) of the Relaxation Peak

Figure 6a–c are the Arrhenius plots of ln f *versus* $1000/T_p$ for $Ti_{50}Ni_{50-x}Cu_x$, x = 0, 5 and 7.5 in cooling/heating, respectively. From Figure 6, the E_a value is calculated; this value is listed in each plot and also in Table 2 for convenient comparison. Table 2 also includes the reported E_a values in $Ti_{50}Ni_{30}Cu_{15}$ [25], $Ti_{50}Ni_{34}Cu_{16}$ [8], $Ti_{50}Ni_{34}Cu_{20}$ [8], and $Ti_{50}Ni_{34}Cu_{25}$ SMAs [25]. Note that in Table 2, the relaxation peak appears in B19' martensite for $x \leq 7.5$, but it occurs in B19 martensite for $x \geq 15$. From Table 2, it is clear that when $x \leq 7.5$, the E_a value is in the range of 0.43~0.69 eV, and it increases as the Cu-content increases, whether in cooling or in heating.

Figure 6. The plots of ln frequency *vs*. reciprocal relaxation peak temperature in cooling and heating processes for $Ti_{50}Ni_{50-x}Cu_x$ SMAs. (**a**) x = 0; (**b**) x = 5; (**c**) x = 7.5 at.%.
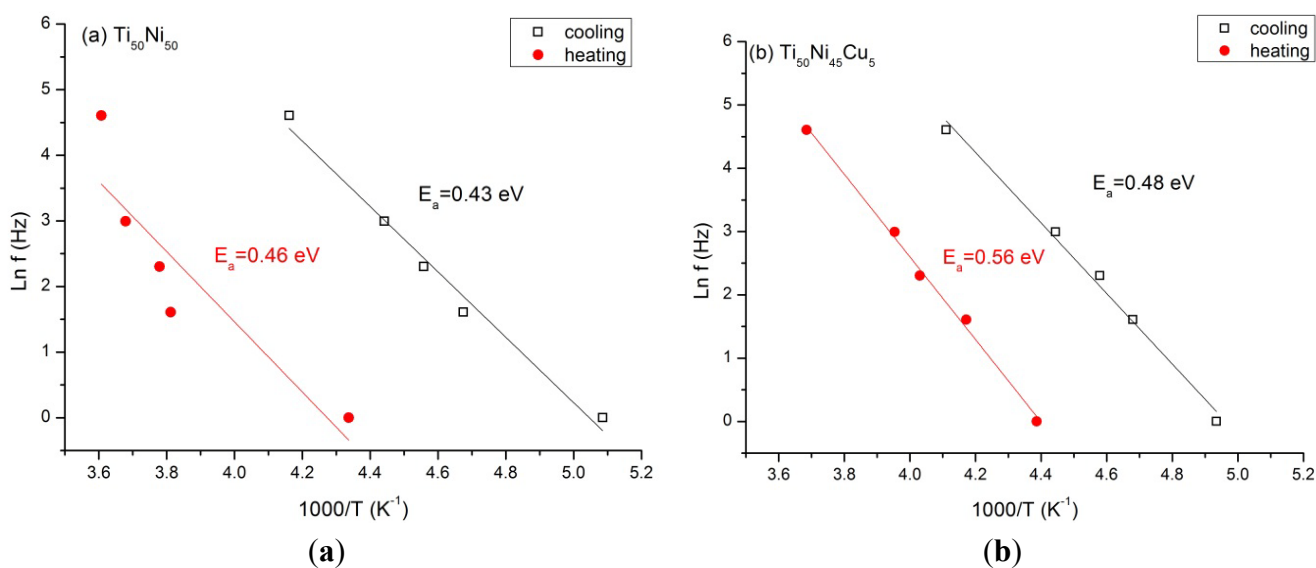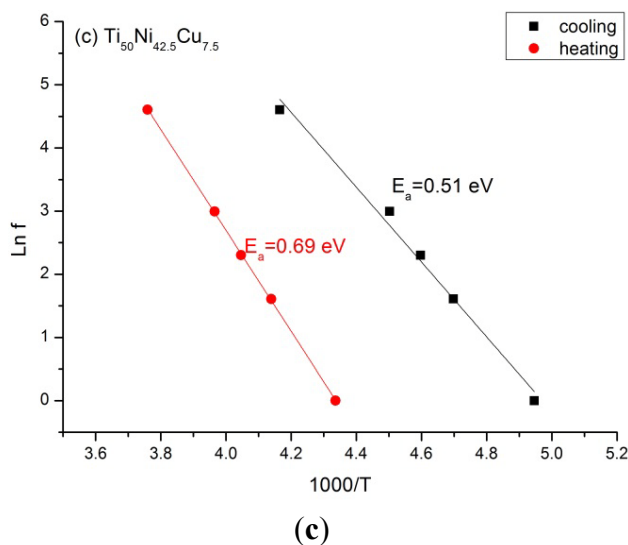
Figure 6. *Cont.*

(c)

Table 2. The activation energy (E_a) values of $Ti_{50}Ni_{50-x}Cu_x$ SMAs determined in cooling and heating processes.

$Ti_{50}Ni_{50-x}Cu_x$, x (at.%)	0 [a]	5 [a]	7.5 [a]	15 [b]	16 [c]	20 [c]	25 [b]
In cooling	0.43 eV	0.48 eV	0.51 eV	N/A	0.76 eV	0.67 eV	N/A
In heating	0.46 eV	0.56 eV	0.69 eV	0.68 eV	0.71 eV	0.64 eV	0.61 eV

a: Data from Figure 5 of this study; b: In Reference [25], SMAs with $x = 15$ and $x = 25$ contained 0.42 and 0.45 at.% H, respectively, after these SMAs were hydrogen-doped; c: In Reference [8], specimens were tested by dual cantilever and step cooling/heating.

However, for $x \geq 15$, the E_a value in cooling/heating is in the range of 0.61~0.76 eV and it doesn't change so much as the Cu-content increases. In addition, the E_a value for $x \geq 15$ is generally larger than that for $x \leq 7.5$. These characteristics of E_a value shown in Table 2 indicate that the effect of the hydrogen atoms pinning the twinned variants in B19' martensite increases as the Cu-contnet increases, and this pinning effect seems to be more significant in B19 martensite than in B19' martensite.

3. Experimental Procedures

$Ti_{50}Ni_{50-x}Cu_x$ ($x = 0, 5, 7.5, 10, 12.5, 15, 20, 25$ and 30 at.%) SMAs were prepared with a vacuum arc remelter (VAR) and homogenized at 900 °C for 4 h. The titanium (purity is 99.7 wt%), nickel (purity is 99.99 wt%), and copper (purity is 99.9 wt%), totaling about 120 g, were remelted six times in an argon atmosphere, which had passed through a gas purifier to reduce its oxygen content. The weight loss during the remelting is less than 1×10^{-4}. For $Ti_{50}Ni_{50-x}Cu_x$ SMAs with $x \leq 12.5$ at.%, the ingots were hot rolled at 900 °C into the plates with a thickness of about 2mm by a rolling machine (DBR150 × 200 2HI-MILL, Daito Seiki Co., Hyogo, Japan), and then solution-heat-treated at 900 °C for 1 h followed by quenching in water, but those with $x = 15$~30 at.% were only solution-heat-treated at 900 °C followed by quenching in water because these SMAs are intrinsically more brittle. The surface oxide layer of the plate/ingot was removed using an etching solution of $HF:HNO_3:H_2O = 1:5:20$ in volume ratio. Thereafter, the plates and the ingots were diamond-saw-cut and spark-cut, respectively,

into specimens with dimensions of $40.0 \times 4.8 \times 1.6$ mm^3 for DMA tests. The damping properties of the specimens were measured with a TA 2980 DMA instrument equipped with a single cantilever and a liquid nitrogen cooling apparatus. The continuous cooling/heating rate was 3 °C/min, and the temperature was ranged from -130 °C to 150 °C. The applied strain and frequency were set at 7.1×10^{-5} and 1 Hz, respectively. From DMA tests, the curves of the tan δ, storage modulus (E_0) and the strain variation values *versus* temperature (T) could all be determined at the same time. For calculating the activation energy (E_a) of the relaxation peak, different frequencies of 0.5, 1, 5, 10, 20 and 100 Hz were employed under a constant strain of 7.1×10^{-5}. The E_a was calculated according to Equation (1):

$$2\pi f \cdot \tau_0 \cdot \exp(E_a/RT_p) = 1 \tag{1}$$

which f is the applied frequency, τ_0 is the relaxation time, R is the gas constant, and T_p is the peak temperature of the relaxation peak in absolute temperature[8].

4. Conclusions

DMA tests at low frequency show that Ti$_{50}$Ni$_{50-x}$Cu$_x$ SMAs exhibit B2 ↔B19' transformation for $x = 0$, 5, 7.5 at.%, B2↔B19↔B19' transformations for $x = 10$, 12.5, 15 at.%, and B2↔B19 transformation for $x = 20$, 25, 30 at.%, in which the transformation hysteresis of B2↔B19' transformation is larger than that of B2↔B19 transformation. The tan δ, storage modulus (E_0) softening/hardening, and strain variation values associated with B2↔B19 transformation are all higher than those with B2↔B19' transformation. The larger E_0 softening/hardening in B2↔B19 can induce higher strain variation in this transformation. It is suggested that the greater mobility of the twin boundaries and the larger magnitude of the strain variation cause the higher tan δ value exhibited in B2↔B19 transformation than in B2↔B19' transformation. The E_0 slope in B19' martensite is much higher than that in B19 martensite, in which the latter is not affected so greatly by changes in temperature, but the former is significantly affected. Relaxation peaks are observed in B19' martensite for $x = 0$, 5, 7.5 at.%, but not in B19 martensite for $x = 20$, 25, 30 at.% because only rare twinned variants are obtained in the B19 martensite. The E_a values of the relaxation peaks are calculated and compared with those reported before, and it is concluded that Ti$_{50}$Ni$_{50-x}$Cu$_x$ SMAs with higher Cu-content possess larger E_a values.

Author Contributions

Miss Chen Chien contributes to the sections of the "experimental procedures" and the "results and discussion" of this paper. Shyi-Kaan Wu contributes to the section of "results and discussion", and he is the principal investigator (PI) of the grants NSC100-2221-E002-100-MY3 and NTU-103R891803. Shih-Hang Chang also contributes to the section of "results and discussion", and he is the principal

Conflicts of Interest

The authors declare no conflict of interest.

References

1. Otsuka, K.; Shimizu, K. Pseudoelasticity and shape memory effects in alloys. *Int. Met. Rev.* **1986**, *31*, 93–114.
2. Miyazaki, S.; Otsuka, K. Development of shape memory alloys. *ISIJ Int.* **1989**, *29*, 353–377.
3. Otsuka, K.; Wayman, C.M. *Shape Memory Materials*; Cambridge University Press: Cambridge, UK, 1998; pp. 1–96.
4. Otsuka, K.; Kakeshita, T. Science and technology of shape-memory alloys: New developments. *MRS Bull.* **2002**, *27*, 91–100.
5. Van Humbeeck, J. Damping capacity of thermoelastic martensite in shape memory alloys. *J. Alloys Compd.* **2003**, *355*, 58–64.
6. Otsuka, K.; Xu, Y.; Ren, X. Ti-Ni-based shape memory alloys as smart materials. *Mater. Sci. Forum* **2003**, *426–432*, 251–258.
7. Otsuka, K.; Ren, X. Physical metallurgy of Ti–Ni-based shape memory alloys. *Prog. Mater. Sci.* **2005**, *50*, 511–678.
8. Fan, G.; Zhou, Y.; Otsuka, K.; Ren, X.; Nakamura, K.; Ohba, T.; Suzuki, T.; Yoshida, I.; Yin, F. Effects of frequency, composition, hydrogen and twin boundary density on the internal friction of $Ti_{50}Ni_{50-x}Cu_x$ shape memory alloys. *Acta Mater.* **2006**, *54*, 5221–5229.
9. Nam, T.H.; Saburi, T.; Shimizu, K. Cu-Content dependence of shape memory characteristics in Ti-Ni-Cu alloys. *Mater. Trans.* **1990**, *31*, 959–967.
10. Nam, T.H.; Saburi, T.; Shimizu, K. Effect of thermo-mechanical treatment on shape memory characteristics in a Ti-40Ni-10Cu (at.%) alloy. *Mater. Trans.* **1991**, *32*, 814–820.
11. Ramachandran, B.; Tang, R.C.; Chang, P.C.; Kuo, Y.K.; Chien, C.; Wu, S.K. Cu-substitution effect on thermoelectric properties of the TiNi-based shape memory alloys. *J. Appl. Phys.* **2013**, *113*, 203702–203707.
12. Chang, S.H.; Hsiao, S.H. Inherent internal friction of $Ti_{50}Ni_{50-x}Cu_x$ shape memory alloys measured under isothermal conditions. *J. Alloys Compd.* **2014**, *586*, 69–73.
13. Teng, Y.; Zhu, S.; Wang, F.; Wu, W. Electronic structures and shape-memory behavior of $Ti_{50}Ni_{50-x}Cu_x$ (x = 0, 6.25, 12.5, 18.75 and 25.0 at.%) by density functional theory. *Phys. B* **2007**, *393*, 18–23.
14. Chang, S.H.; Wu, S.K. Textures in cold-rolled and annealed $Ti_{50}Ni_{50}$ shape memory alloy. *Scripta Mater.* **2004**, *50*, 937–941.
15. San, J.; Nó, M.L. Damping behavior during martensitic transformation in shape memory alloys. *J. Alloys Compd.* **2003**, *355*, 65–71.
16. Chen, Y.; Jiang, H.C.; Liu, S.W.; Rong, L.J.; Zhao, X.Q. Damping capacity of TiNi-based shape memory alloys. *J. Alloys Compd.* **2009**, *482*, 151–154.

17. Chien, C.; Wu, S.K. Damping capacities of $Ti_{50}Ni_{50-x}Cu_x$ shape memory alloys measured under temperature, strain, and frequency sweeps. In Proceedings of International Conference on Electronic Materials, Taipei, Taiwan, 10–14 June 2014.

18. Lo, Y.C.; Wu, S.K.; Horng, H.E. A study of B2↔B19↔B19' two-stage martensitic transformation in a $Ti_{50}Ni_{40}Cu_{10}$ alloy. *Acta Metall. Mater.* **1993**, *41*, 747–759.

19. Yoshida, I.; Monma, D.; Iino, K.; Otsuka, K.; Asai, M.; Tsuzuki, H. Damping properties of $Ti_{50}Ni_{50-x}Cu_x$ alloys utilizing martensitic transformation. *J. Alloys Compd.* **2003**, *355*, 79–84.

20. Lin, K.N.; Wu, S.K. Multi-stage transformation in annealed Ni-rich $Ti_{49}Ni_{41}Cu_{10}$ shape memory alloy. *Intermetallics* **2010**, *18*, 87–91.

21. Nagasawa, A.; Nakanishi, N.; Enami, K. The nature of special-mode softening and the mechanism of martensitic phase transition in β-phase alloys. *Philos. Mag. A* **1981**, *43*, 1345–1357.

22. Ren, X.; Taniwaki, K.; Otsuka, K.; Suzuki, T.; Tanaka, K.; Chumlyakov, Y.I.; Ueki, T. Elastic constants of $Ti_{50}Ni_{30}Cu_{20}$ alloy prior to martensitic transformation. *Philos. Mag. A* **1999**, *79*, 31–41.

23. Chang, S.H.; Wu, S.K. Determining transformation temperatures of equiatomic TiNi shape memory alloy by dynamic mechanical analysis test. *J. Alloys Compd.* **2013**, *577*, S241–S244.

24. Jiang, H.J.; Ke, C.B.; Cao, S.S.; Ma, X.; Zhang, X.P. Phase transformation and damping behavior of lightweight porous TiNiCu alloys fabricated by powder metallurgy process. *Trans. Nonferr. Met. Soc. China* **2013**, *23*, 2029–2036.

25. Ueura, T.; Sakaguchi, T.; Igata, N.; Takeuchi, S. Internal friction of hydrogenated Ti (Ni, Cu) shape memory alloys. *Key Eng. Mater.* **2006**, *319*, 39–44.

26. Tadaki, T.; Wayman, C.M. Electron microscopy studies of martensitic transformations in $Ti_{50}Ni_{50-x}Cu_x$ alloys. Part I. Compositional dependence of one-third reflections from the matrix phase. *Metallography* **1982**, *15*, 233–245.

27. Tadaki, T.; Wayman, C.M. Electron microscopy studies of martensitic transformations in $Ti_{50}Ni_{50-x}Cu_x$ alloys. Part II. Morphology and crystal structure of martensites. *Metallography* **1982**, *15*, 247–258.

28. Moberly, W.; Proft, J.; Duerig, T. Twinless martensite in TiNiCu shape memory alloys. *Mater. Sci. Forum* **1990**, *56–58*, 605–610.